THE ASTROPHYSICAL JOURNAL, 633:L133–L136, 2005 November 10


# THE 10 μm FEATURE OF M-TYPE STARS IN THE LARGE MAGELLANIC CLOUD AND THE DUST CONDENSATION SEQUENCE[1]

C. DIJKSTRA, A. K. SPECK, AND R. B. REID
Department of Physics and Astronomy, University of Missouri, Columbia, MO 65211; dijkstrac@missouri.edu
AND
P. ABRAHAM
Konkoly Observatory, P.O. Box 67, H-1525 Budapest, Hungary
*Received 2005 September 13; accepted 2005 September 29; published 2005 October 21*

## ABSTRACT

We present 7–14 μm *Infrared Space Observatory* (*ISO*) spectroscopy of 12 M-type evolved stars in the Large Magellanic Cloud (LMC), in order to study the dust mineralogy and condensation process around these stars. The sample stars show a broad dust feature in the 7–14 μm region, which is seen in either emission or (self-) absorption. The shape of the feature changes with increasing mass-loss rate, $\dot{M}$, suggesting a change in dust mineralogy as the central star evolves. At low mass-loss rates amorphous alumina and amorphous silicates are observed, while at high mass-loss rates only amorphous silicates are seen, in agreement with the classical condensation sequence expected for these materials. We find a clear correlation between $\dot{M}$ and the peak wavelength position of the broad dust feature. Our data suggest a strong dependence of the dust mineralogy on the temperature at the dust condensation radius.

*Subject headings:* circumstellar matter — infrared: stars — stars: AGB and post-AGB — stars: late-type — stars: mass loss — stars: winds, outflows

## 1. INTRODUCTION

Asymptotic giant branch (AGB) and red supergiant (RSG) stars are the highly evolved descendants of low- to intermediate- ($1\ M_\odot \le M < 8\ M_\odot$) and high-mass ($M \ge 8\ M_\odot$) stars, respectively. These stars are luminous cool giants, which lose mass at high rates ($10^{-7}$ to $\sim 10^{-3}\ M_\odot\ \mathrm{yr}^{-1}$). The mass-loss rate is expected to increase over time (e.g., Lattanzio & Wood 2004; van Loon et al. 2005). Mass loss leads to the formation of a circumstellar envelope, in which dust particles form in the outflowing gas and help drive mass loss. The subsequent appearance of different dust species from the outflowing gas is known as the "dust condensation sequence." The order in which condensation of different species occurs depends on the physical conditions within the envelope and is still poorly understood. Around M-type stars, which have oxygen-rich atmospheres (C/O < 1), oxides and silicates are expected to form (e.g., Tielens 1990; Tielens et al. 1997). Here amorphous alumina (an oxide) and amorphous silicates may show broad spectral features near 10 μm (see, e.g., Speck et al. 2000).

In this Letter we present the 7−14 μm *Infrared Space Observatory* (*ISO*; Kessler et al. 1996) spectra of 12 M-type AGB and RSG stars in the Large Magellanic Cloud (LMC). We study their 10 μm features (defined in § 3) and the dust condensation sequence around these stars as a function of their (circum)stellar parameters. In § 2 we present the *ISO* spectra, followed by a description and discussion of our results in § 3.

## 2. OBSERVATIONS

Figure 1 shows the 7–14 μm *ISO* spectra of our sample stars. The spectra were observed using the *ISO* Camera (ISOCAM, 2.5–18 μm; Cesarsky et al. 1996) and Imaging Photo-Polarimeter (PHT, 2.5–11.6 μm; Lemke et al. 1996); the ISOCAM observations were first published by Trams et al. (1999). The PHT data were taken with its spectrophotometric subsystem, PHT-S, and reduced using the ISOPHOT Interactive Analysis tool (PIA; Gabriel et al. 1997). Here we used pipeline version OLP 10 data from the *ISO* data archive. We applied standard reduction techniques, including two-threshold deglitching, orbital-dependent dark current subtraction, and dynamic response calibration. Postprocessing was also applied, which included additional deglitching, zodiacal background subtraction, and empirical photometric correction. Memory and off-center corrections were applied to individual sources when applicable. Table 1 summarizes which data were used for each star.

Also shown in Figure 1 are spline-fit continua for the *ISO* spectra, which have been determined following a method outlined by Molster et al. (2002). Each continuum is required to be smooth and to maximize the continuum flux. It is used only to enhance the visibility of sharp features in the spectrum and has no physical meaning. Note that the continua where determined using a larger wavelength range than shown here. The spectra and continua for Mira and W Hya, which are Galactic sources, where taken from Speck et al. (2000) and serve as comparison objects.

## 3. RESULTS AND DISCUSSION

In Figure 2 we plot the continuum-divided spectra of our sample stars as a function of increasing mass-loss rate, $\dot{M}$, which is listed in Table 1 and taken from van Loon et al. (1999). The sample stars show a broad dust feature in the 7–14 μm region (hereafter the 10 μm feature), which is seen either in emission or (self-)absorption. The shape of the 10 μm feature changes with increasing $\dot{M}$, suggesting a change in dust mineralogy as the central star evolves.

Figure 2 also shows the continuum-divided spectra of W Hya and Mira (not necessarily ordered according to an increasing $\dot{M}$). The spectrum of W Hya is representative for a mixture of amorphous alumina ($Al_2O_3$), an oxide, and amorphous olivine ($MgFeSiO_4$), a silicate, while that of Mira is attributed to amorphous silicates (Speck et al. 2000). It can be seen that, at

[1] Based on observations with *ISO*, an ESA project with instruments funded by ESA Member States (especially the PI countries: France, Germany, the Netherlands and the UK) and with the participation of ISAS and NASA.

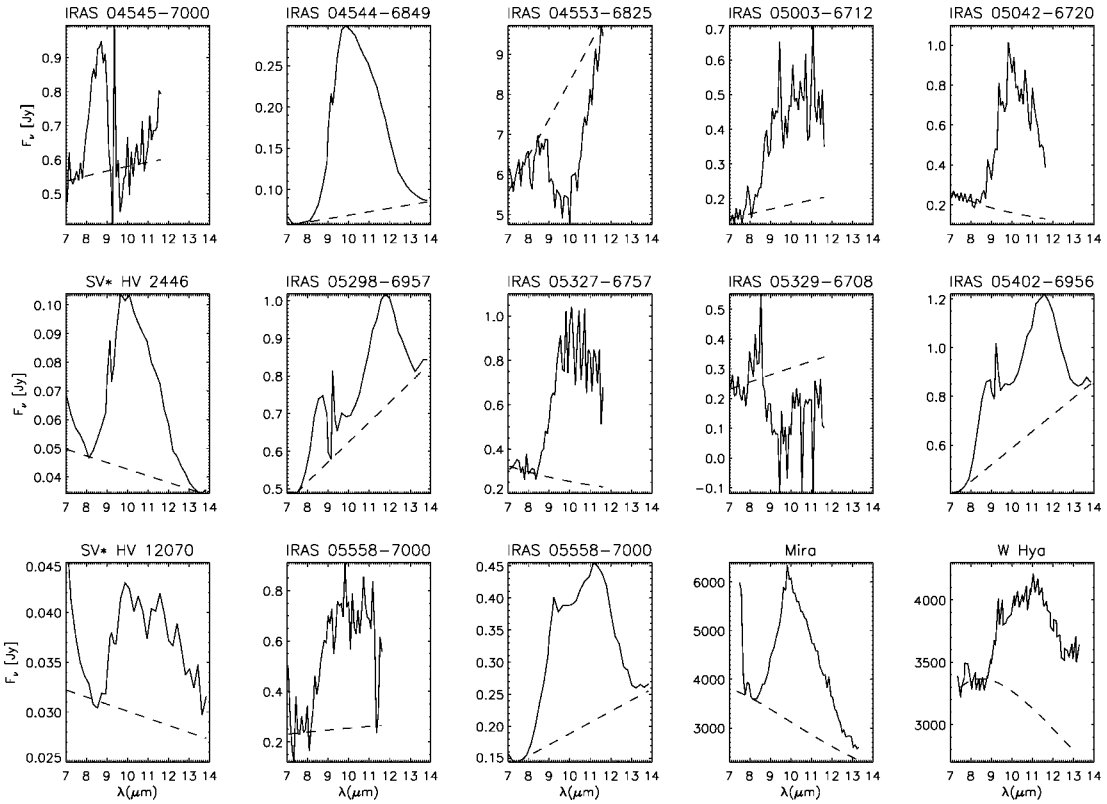


FIG. 1.—*ISO* spectra of the sample stars and their continua (*dashed lines*). For details see § 2.

low mass-loss rates, the 10 $\mu$m feature of the LMC stars most closely resembles that of W Hya. As mass loss increases, the 10 $\mu$m feature shifts to shorter wavelengths, more closely resembling that of Mira, and eventually goes into self-absorption. We thus find that with increasing mass-loss rate the dust mineralogy changes from an amorphous alumina and amorphous olivine mixture into an amorphous silicate–only composition.

This is in agreement with the classical condensation sequence proposed for these materials by Tielens (1990). Depending on the density distribution in the envelope, the condensation sequence stops at different points in the envelope (Tielens 1990; Tielens et al. 1997). If the density drops rapidly with distance from the star, only various oxides (including $Al_2O_3$) are expected to form close to the star. If densities are somewhat higher farther out in the envelope, Ca-Al silicates may also form through gas-grain reactions. If densities are higher still further out, Mg silicates may also form as mantles on the Ca-Al silicates. An increasing $\dot{M}$ provides increasing densities in the envelope. Therefore, while at low $\dot{M}$ the mineralogy may be expected to be dominated by oxides, it will become increasingly dominated by silicates as $\dot{M}$ increases, naturally accounting for the trend in Figure 2.

Alternatively, Stencel et al. (1990) hypothesized the formation of chaotic silicates, in which Al-O bonds form at the expense of Si-O bonds. From this Sloan & Price (1998) concluded that less-evolved stars with low C/O ratios should show

TABLE 1

DETAILS OF THE *ISO* OBSERVATIONS AND DERIVED (CIRCUM)STELLAR PARAMETERS.

| No. (1) | *IRAS* Name (2) | Data (3) | TDT No. (4) | $T_{\rm eff}$[a] (K) (5) | $R_b$[a] ($R_\odot$) (6) | $R_{\rm in}$[a] ($R_*$) (7) | $\dot{M}$[a] ($10^{-6}\ M_\odot\ {\rm yr}^{-1}$) (8) | log ($\rho_c$ [g cm$^{-3}$]) (9) | log ($T_c$ [K]) (10) | log ($P_c$ [bar]) (11) | $\lambda_{10}$[b] ($\mu$m) (12) |
|---|---|---|---|---|---|---|---|---|---|---|---|
| 1 ..... | 04545−7000 | PHT | 15700828 | 2890 | 850 | 12.0 | 280 | −14.731 | 2.921 | −4.255 | 9.94 |
| 2 ..... | 04544−6849 | CAM | 75600751 | 2890 | 700 | 8.0 | 7 | −15.812 | 3.009 | −5.248 | 9.92 |
| 3 ..... | 04553−6825 | PHT | 19100531 | 3126 | 2100 | 16.0 | 2800 | −14.767 | 2.893 | −4.319 | 9.81 |
| 4 ..... | 05003−6712 | PHT | 19100438 | 2890 | 560 | 9.5 | 29 | −15.150 | 2.972 | −4.623 | 10.31 |
| 5 ..... | 05042−6720 | PHT | 15701116 | 3574 | 1300 | 15.5 | 5 | −17.071 | 2.958 | −6.558 | 10.33 |
| 6 ..... | SV* HV 2446 | CAM | 71601724 | 3434 | 540 | 13.3 | 1.5 | −16.697 | 2.974 | −6.169 | 10.13 |
| 7 ..... | 05298−6957 | CAM | 69101729 | 2890 | 800 | 12.0 | 230 | −14.764 | 2.921 | −4.288 | 10.07 |
| 8 ..... | 05327−6757 | PHT | 12500132 | 3574 | 950 | 16.5 | 13 | −16.437 | 2.944 | −5.938 | 10.34 |
| 9 ..... | 05329−6708 | PHT | 12500285 | 2890 | 600 | 12.0 | 180 | −14.620 | 2.921 | −4.144 | 9.45 |
| 10 ..... | 05402−6956 | CAM | 74401132 | 2890 | 550 | 12.0 | 180 | −14.545 | 2.921 | −4.069 | 10.04 |
| 11 ..... | SV* HV 12070 | CAM | 74901933 | 3309 | 600 | 11.2 | 0.5 | −17.117 | 2.995 | −6.567 | 10.90 |
| 12 ..... | 05558−7000 | PHT | 17100395 | 2890 | 750 | 9.8 | 50 | −15.195 | 2.965 | −4.674 | 9.73 |
| 13 ..... | 05558−7000 | CAM | 74300934 | 2890 | 480 | 10.5 | 50 | −14.867 | 2.950 | −4.362 | 10.20 |

NOTE.—Parameters are defined in §§ 2 and 3. If no *IRAS* name (col. [2]) exists for a given source, an alternative is given. A TDT number (col. [4]) uniquely identifies an *ISO* observation in the *ISO* data archive.

[a] Data taken from van Loon et al. (1999).

[b] $\lambda_{10}$ is the peak wavelength position of the 10 $\mu$m feature (see § 3).

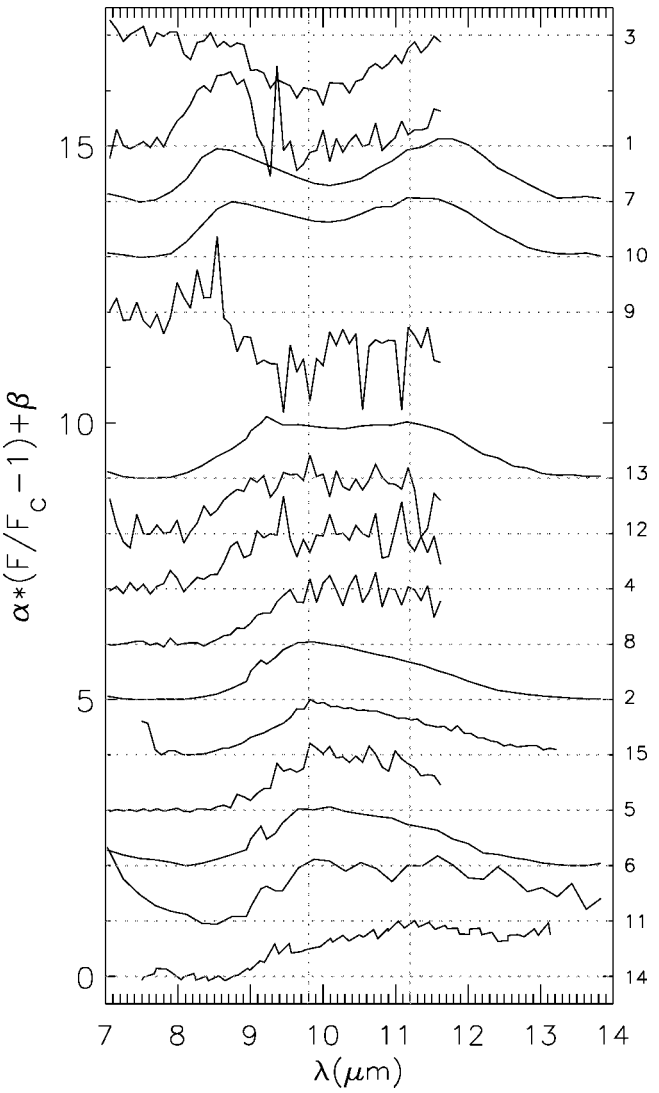


FIG. 2.—Continuum-divided spectra ($F/F_c$) for the stars in Fig. 1 as a function of increasing mass-loss rate ($\dot{M}$ increases from bottom to top). The spectra are normalized and offset for clarity. Horizontal and vertical dotted lines indicate continuum levels and the peak wavelength positions for Mira (9.8 $\mu$m) and W Hya (11.2 $\mu$m). Numbers are those listed in Table 1; 14 is W Hya, and 15 is Mira. An artifact near 9 $\mu$m in the spectra of Fig. 1 has been removed from the spectra plotted here.

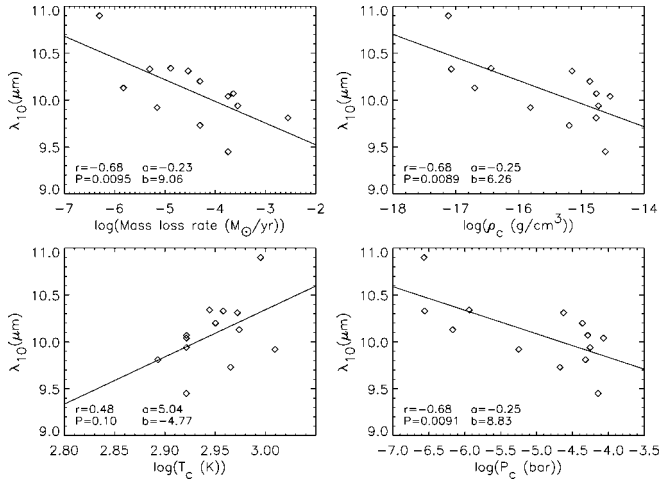


FIG. 3.—Plots of $\lambda_{10}$ as a function of $\log \dot{M}$, $\log \rho_c$, $\log T_c$, and $\log P_c$. A correlation coefficient ($r$), its two-sided significance ($P$), and least-squares fitting coefficients (slope $a$, offset $b$) are given in the lower left part of each panel.

silicate features, while more-evolved stars with higher C/O ratios should show $Al_2O_3$-dominated spectra. Noting that $\dot{M}$ also increases as the stars evolves, our results clearly contradict this scenario.

In Figure 3 we plot the peak wavelength position of the 10 $\mu$m feature, $\lambda_{10}$, which was estimated by eye and is assumed to be a measure for the dust mineralogy, as a function of $\dot{M}$, and the mass density, $\rho_c$, temperature, $T_c$, and pressure, $P_c$, at the dust condensation radius, $R_{in}$. Here, $\rho_c$, $T_c$, and $P_c$ were calculated from $\dot{M}$, $R_{in}$, and the effective temperature, $T_{eff}$, and radius, $R_b$, of the central star, derived through detailed radiative transfer modeling of our *ISO* spectra by van Loon et al. (1999). Furthermore, we assumed a gas outflow velocity of $v_{gas} = 15$ km s$^{-1}$, and a $T(R) \propto R^{-0.5}$ temperature distribution, where $R$ is the distance to the central star. This temperature distribution serves as an estimate only. It assumes an optically thin envelope, which may be invalid for high mass-loss rates. Finally, we assumed a mean molecular weight of $\mu = 2.3 m_p$ for the gas, where $m_p$ is one proton mass and it is assumed that all H is in $H_2$ and that $H_2$ and He are the dominant gas species (Dijkstra et al. 2003). Table 1 summarizes the calculations and measurements.

Least-squares fitting (Fig. 3) suggests an approximately $\dot{M}^{-0.23}$ dependence of $\lambda_{10}$ on $\dot{M}$, indicating the previously discussed change in dust mineralogy with mass-loss rate. This probably explains the similar $\rho_c^{-0.25}$ dependence of $\lambda_{10}$. The correlation between $\lambda_{10}$ and $\dot{M}$ and $\rho_c$ is strong (Fig. 3; we find high correlation coefficients, $r$, and low two-sided significances, $P$). Furthermore, there appears to be a very strong, approximately $T_c^5$, dependence of $\lambda_{10}$ on $T_c$, although the correlation between $\lambda_{10}$ and $T_c$ is less clear (Fig. 3; we find a lower $r$ and higher $P$ value). The latter may be due to the fact that $T_c$ covers a relatively narrow range of values (~800–1000 K) compared to $\rho_c$ (which covers ~3–4 orders of magnitude), making it more difficult to establish a clear relation in case of $T_c$.

We find that the dust mineralogy (when measured by $\lambda_{10}$) depends strongly on the temperature at the dust condensation radius. In contrast, the dependence on the mass density at this radius is much weaker. The strong temperature dependence supports the thermodynamic condensation sequence described by Tielens (1990), and can be explained by the fact that in order to form grains, nucleation sites (seeds) are needed. The ease with which these are formed is mainly determined by the temperature (Gail & Sedlmayr 1999). We speculate that once seeds have been formed, the mass density at the dust condensation radius become more important for the dust mineralogy than the temperature. This is based on the work of Gail & Sedlmayr (1999), who show that for grain at rest with respect to the gas phase, its growth rate, which strongly influences the observed dust mineralogy, is proportional to $Z_{gr} \propto \rho_c \sqrt{T_c}$. Here we ignore decomposition of the grain by chemical reactions (Gail & Sedlmayr 1999).

If correct, the above scenario could provide a clue as to the apparent absence of pure $Al_2O_3$ in the spectra of Figure 2. According to Tielens (1990), $Al_2O_3$ condenses first from the gas phase, and is consequently difficult to form. Next silicates form on the $Al_2O_3$ seed by the addition of gas-phase SiO, Mg, and Fe and consequent chemical reactions (Gail & Sedlmayr 1999). Since this process is more sensitive to the mass density than the temperature, however, it should proceed far more

efficiently. As a result, some silicate grains are always present. At low densities (low $M$), the $Al_2O_3$ is not completely hidden, and thus we see a mixture of $Al_2O_3$ and silicates. At high densities (high $M$), the $Al_2O_3$ is efficiently coated and the silicate feature dominates.

Finally, we note that van Loon et al. (1999) assumed an amorphous olivine (i.e., amorphous silicate) composition for all our sample stars while deriving their (circum)stellar parameters. We expect this assumption to have a minor effect on our analysis, in particular for the silicate-dominated sources. Still, for those objects showing a mixture of $Al_2O_3$ and silicates, in principle two dust condensation radii must be specified, since the two materials condense at different temperatures. Here, our adopted dust condensation radius for $Al_2O_3$ is thus too large, since $Al_2O_3$ condenses at a higher temperature than silicates do. Therefore, $\rho_c$, $T_c$, and $P_c$ for the more $Al_2O_3$-dominated sources in Figure 3 (i.e., those with larger $\lambda_{10}$ values) should be larger. As a result, the dependence of the dust mineralogy (as measured by $\lambda_{10}$) on temperature weakens, whereas the dependence on density (and pressure) becomes stronger. However, despite this effect, we expect the dependence on temperature to remain stronger than the dependence on density.

This work was supported by the NASA Astrophysical Data Program (NAG 5-12675) and the University of Missouri Research Board. We thank J. T. van Loon for providing the ISOCAM data, and are grateful to I. Izouimine for his software support, which was necessary for our data analysis. The ISOPHOT data presented in this Letter were reduced using PIA, which is a joint development by the ESA Astrophysics Division and the ISOPHOT Consortium with the collaboration of the Infrared Processing and Analysis Center (IPAC). Contributing ISOPHOT Consortium institutes are DIAS, RAL, AIP, MPIK, and MPIA.

REFERENCES

Cesarsky, C. J., et al. 1996, A&A, 315, L32
Dijkstra, C., Dominik, C., Hoogzaad, S. N., de Koter, A., & Min, M. 2003, A&A, 401, 599
Gabriel, C., Acosta-Pulido, J., Heinrichsen, I., Morris, H., & Tai, W. M. 1997, in ASP Conf. Ser. 125, Astronomical Data Analysis Software and Systems VI, ed. G. Hunt & H. E. Payne (San Francisco: ASP), 108
Gail, H.-P., & Sedlmayr, E. 1999, A&A, 347, 594
Kessler, M. F., et al. 1996, A&A, 315, L27
Lattanzio, J. C., & Wood, P. R. 2004, in Asymptotic Giant Branch Stars, ed. H. J. Habing & H. Olofsson (New York: Springer), 23
Lemke, D., et al. 1996, A&A, 315, L64
Molster, F. J., Waters, L. B. F. M., Tielens, A. G. G. M., & Barlow, M. J. 2002, A&A, 382, 184
Sloan, G. C., & Price, S. D. 1998, ApJS, 119, 141
Speck, A. K., Barlow, M. J., Sylvester, R. J., & Hofmeister, A. M. 2000, A&AS, 146, 437
Stencel, R. E., Nuth, J. A., Little-Marenin, I. R., & Little, S. J. 1990, ApJ, 350, L45
Tielens, A. G. G. M. 1990, in From Miras to Planetary Nebulae: Which Path for Stellar Evolution?, ed. M. O. Mennessier & A. Omont (Gif-sur-Yvette: Editions Frontières), 186
Tielens, A. G. G. M., Waters, L. B. F. M., Molster, F. J., & Justtanont, K. 1997, Ap&SS, 255, 415
Trams, N. R., et al. 1999, A&A, 346, 843
van Loon, J. T., Cioni, M.-R. L., Zijlstra, A. A., & Loup, C. 2005, A&A, 438, 273
van Loon, J. T., et al. 1999, A&A, 351, 559